Arginine-Mediated Self-Assembly of Porphyrin on Graphene: A Photocatalyst for Degradation of Dyes

Duong Duc La [1], Rahul V. Hangarge [1], Sidhanath V. Bhosale [2], Ha Duc Ninh [4], Lathe A. Jones [1,3] and Sheshanath V. Bhosale [1,*

[1] School of Science, RMIT University, GPO BOX 2476, Melbourne, VIC-3001, Australia; duc.duong.la@gmail.com (D.D.L.); rahulhangarge86@gmail.com (R.V.H.); lathe.jones@rmit.edu.au (L.A.J.)

[2] Polymers and Functional Material Division, CSIR-Indian Institute of Chemical Technology, Hyderabad 500 007, Telangana, India; sidhanath.bhosale@gmail.com

[3] Centre for Advanced Materials and Industrial Chemistry (CAMIC), RMIT University, GPO BSOX 2476, Melbourne, VIC-3001, Australia

[4] Institute of Chemistry & Materials Science, 17 Hoang Sam, Hanoi 100000, Vietnam; ninhducha1974@gmail.com

[*] Correspondence: sheshanath.bhosale@rmit.edu.au or bsheshanath@gmail.com; Tel.: +61-03-25-2680

Featured Application: photocatalyst for degradation of dyes.

Abstract: Porphyrin nanostructures with well-controlled size, shape and functionality can be used for visible-light photocatalysis. In this work, a graphene@porphyrin nanofibre composite was successfully fabricated via arginine-mediated self-assembly of tetrakis (4-carboxyphenyl) porphyrin (TCPP) on graphene nanoplates (GNPs). The formation and crystallisation of the graphene@porphyrin nanofibre composite was fully characterized by scanning electron microscopy (SEM), transmission electron microscopy (TEM), X-ray diffraction (XRD), fourier transform infrared (FTIR), ultraviolet-visible (UV-vis) and fluorescence spectroscopy. The assembled TCPP nanofibers were 50–200 nm in diameter with length in micrometers long, which were densely and uniformly distributed on the surface of graphene. The GNPs@TCPP nanofibers showed enhanced visible-light photocatalytic activity in comparison with free-standing TCPP nanorods for the degradation of Rhodamine B (RhB) and methyl orange (MO). The possible photodegradation mechanism of these dyes by the GNPs@TCPP nanofiber photocatalyst was proposed.

Keywords: tetrakis (4-carboxyphenyl) porphyrin; self-assembly; photocatalyst; dyes degradation; pollutant treatment; graphene nanoplates

1. Introduction

Supramolecular self-assembly of porphyrin-based materials has attracted intensive interest from scientists as an effective protocol to design functional structures during the past decade [1–3]. π-Conjugated porphyrins have been extensively studied as building blocks for the construction of solid-state nanostructured materials [4–8], which can be utilized in many applications such as optoelectronic nanodevices, energy storage, catalysis, photodynamic therapy, sensors and photonics [9–13]. Supramolecular nanostructures via self-assembly are usually produced via non-covalent interactions such as hydrogen bonding, electrostatic, van der Waals interactions, π–π interactions, and coordination. These soft materials are fabricated by self-assembly protocols including ionic self-assembly [14], surfactant-assisted self-assembly (SAS) [15], and reprecipitation [16,17]. Many well-defined and controlled nanostructures such as nanoprisms, nanotubes, nanofibre bundles, nanorods, nanosheets, nanospheres, nanoclovers, nanowires and nanoparticles have thus been

reported [14,16,18–22]. Recently; visible-light photocatalytic applications of self-assembled porphyrin nanostructures have been extensively reported [23–25]. Zhong and colleagues reported the dependence of photocatalytic performance on various hierarchically structured porphyrin nanocrystals such as nanosheets, octahedrons and microspheres [26]. More recently, we successfully fabricated porphyrin nanobelts via arginine-induced self-assembly of tetrakis (4-carboxyphenyl) porphyrin (TCPP), and used the structure for the photodegradation of model pollutant Rhodamine B (RhB) under visible-light irradiation [27,28].

Graphene, due to its large surface area, high number of adsorption sites, and good charge transfer properties has been demonstrated to be a good platform for semiconductor materials to enhance the photocatalytic activity [29–36]. However, only a few studies have been reported so far on combination of porphyrin nanostructures with the graphene for photocatalytic applications. For example, Chen et al. employed vacuum filtration methods to integrate porphyrin nanoparticles into reduced graphene oxide (RGO) for use in photocatalysis [24]. In another study, Guo's group studied visible-light photocatalytic activity of a one-dimensional porphyrin formed by self-assembly assisted by graphene oxide [37]. However, these studies faced disadvantages, being poor integration or poor distribution of the porphyrin nanostructures on the graphene substrate. Recently, we reported well-dispersed TCPP nanorods on graphene for enhanced photocatalytic performances [38].

Herein, we fabricate a graphene nanoplates (GNPs)@porphyrin nanofiber composite via arginine-mediated reprecipitation of TCPP on the graphene surface, and use the material as a photocatalyst for degradation of a dye.

2. Materials and Methods

2.1. Materials

All chemicals were used as received without any further purification. D-Arginine was obtained from Sigma Aldrich (Bengaluru, Karnataka, India) and graphene nanoplates (GNPs) were purchased from VNgraphene (Hanoi, Vietnam). Chemicals such as dry acetone, propionic acid, dichloromethane, chloroform, sodium hydroxide (NaOH), methyl orange (MO), Rhodamine B (RhB), potassium hydroxide (KOH) and ethanol were purchased from Ajax Finechem (Melbourne, Australia).

2.2. Synthesis of H_2TCPP

H_2TCPP was synthesized by a literature procedure [39] and was characterized by standard spectroscopic methods.

2.3. Arginine-Mediated Self-Assembly of TCPP on the Graphene Surface

First, 8 mg of TCPP and 4 mg of GNPs were dissolved and sonicated in 1 mL of 0.2 M NaOH solution for 15 min. This is assigned as the guest solution. The host solution was prepared by dissolving 16 mg of D-arginine in 20 mL of 0.01 M HCl solution. Subsequently, the guest solution was added dropwise into the host solution under stirring at room temperature in the dark for 1 h. The obtained dark green aggregates (GNPs@TCPP nanofibers) were then filtered and dried for further characterizations (Figure 1).

2.4. Photocatlytic Investigation

Photocatalytic performance of the GNPs@TCPP nanofibers was evaluated by the degradation of RhB and MO in aqueous solution. In a typical photodegradation measurement, 0.1 mg of composite was dispersed in a 20 mL aqueous solution of dye with a concentration of 5 mg L^{-1}. The dispersion was stirred for 30 min and left overnight in the dark to establish an adsorption/desorption equilibrium before irradiation. The simulated sunlight source for the photocatalytic reaction was a 1500 W air-cooled Xenon lamp. At appointed times, 1.5 mL of dispersion aliquots were taken out and centrifuged to remove photocatalyst. The photocatalytic performance of the as-fabricated samples for

dyes degradation was evaluated by recording the real-time absorptivity at a wavelength of 553 nm for RhB and 446 nm for MO.
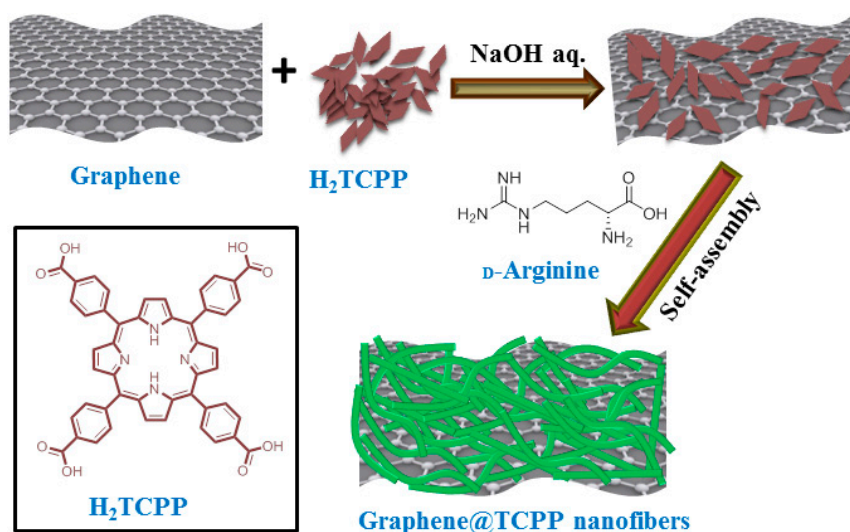

Figure 1. Schematic diagram of arginine-mediated self-assembly of porphyrin nanofibers on graphene surface.

2.5. Characterization

The supramolecular self-assembled nanostructure morphology of GNPs@TCPP nanofiber were studied by scanning electron microscopy (SEM) using an FEI Nova NanoSEM instrument (FEI, Hillsboro, OR, USA, operating under high-voltage and Stage bias condition of 15 KeV with Pt coating). Transmission electron microcopy (TEM) samples were prepared and measured by paper blotting method followed by solvent evaporation on a holey carbon coated copper grid. The micrographs were investigated using a Jeol 1010 100 kV transmission electron microscope (JEOL, Peabody, MA, USA). Ultraviolet-visible (UV-vis) absorption measurements of samples in solution and in solid-state were carried out using a Cary 50 Bio spectrophotometer with a cell of 1 cm path length. Furthermore, UV-vis absorption measurements were also employed to record the photocatalytic performance for dyes degradation. Horiba JobinYvonFluoroMax-4 spectrofluorometer (Horiba, Kyto, Japan) was used to record fluorescence emission spectra of obtained materials. All experiments were performed in a quartz cell with a 1 cm path length upon excitation at 420 nm wavelength. A BrukerAXS D8 Discover instrument (Billerica, MA, USA) with a general area detector diffraction system (GADDS) using a Cu Kα source was utilized to obtain X-ray diffraction (XRD) patterns of GNPs@TCPP nanofibers.

3. Results

Figure 2A shows the SEM image of GNPs obtained from VNgraphene. It is clear that the GNPs have a wrinkled, crumpled structure with a lateral diameter of tens of microns. The semitransparency of GNPs to the electron beam also suggests that the thickness of GNPs is approximately 5–15 nm [40]. Figure 2B is the SEM image of free-standing arginine-mediated self-assembly of porphyrins dropped onto a silicon wafer. The assembled porphyrins have similar morphology to our previous work [27], which is best described as a belt-like morphology several microns in length, with diameters of about 20–30 nm.
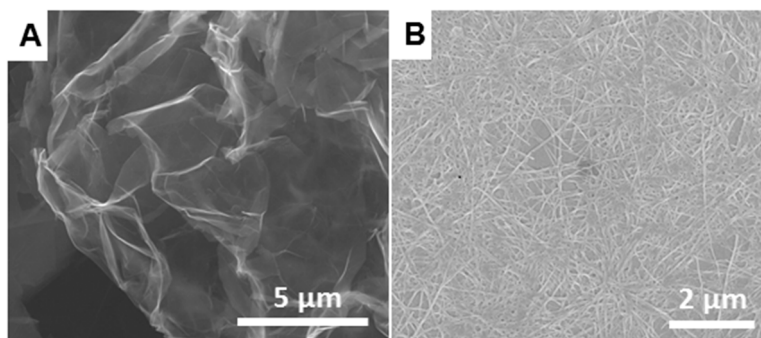
Figure 2. Scanning electron microscopy (SEM) images of (**A**) graphene nanoplates, (**B**) free-standing arginine-induced tetrakis (4-carboxyphenyl) porphyrin (TCPP) aggregates.

The morphology and distribution of the arginine-mediated self-assembly porphyrin TCPP on the graphene are observed by SEM and TEM images in Figure 3, Figures S1 and S2. It is seen that the porphyrins nanofibers were densely and uniformly distributed on the surface of the GNPs with a diameter ranging from 50 to 200 nm and several micrometers in length. In contrast to Arginine-assisted self-assembly of TCPP with GNPs, which demonstrated the formation of well-dispersed porphyrin nanorods with 50–100 nm in diameter and about 200 nm in length on the GNPs surface [38], in this case the diameter of the TCPP aggregates are almost unchanged. This suggests that the presence of arginine helps to elongate the aggregation of TCPP to form nanofibers with length on the micron scale.
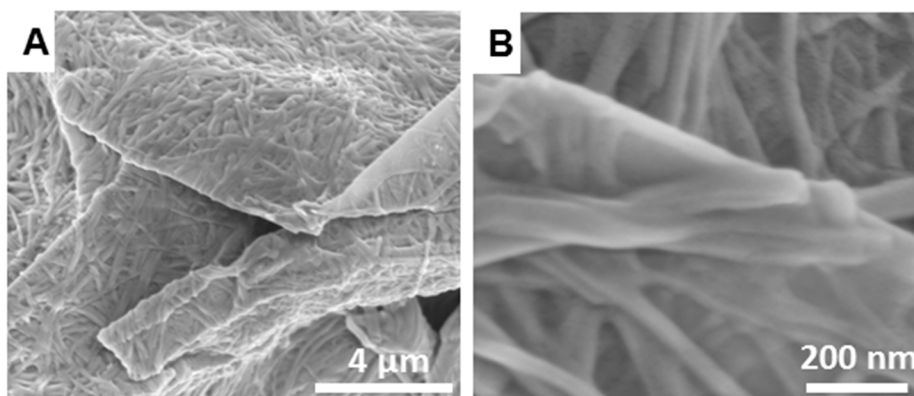

Figure 3. (**A**) Low and (**B**) high-resolution SEM images of arginine-induced self-assembly of TCPP on the graphene surface, respectively.

Figure 4A shows the UV-vis spectra of monomeric TCPP molecules, free-standing TCPP aggregates and GNPs@TCPP nanofibers. The absorption spectrum of the TCPP monomer shows a strong peak at 414 nm, namely a Soret absorption, as a result of a transition from a_{1u} (π) to e^{*}_{g} (π), and four weak peaks ranging from 500 to 700 nm, which are ascribed to Q bands of the a_{2u} (π) to e^{*}_{g} (π) transition [24,41]. Free-standing TCPP aggregates in the presence of arginine reveal a Soret absorption peak at 417 nm and the four weak absorption peaks of Q bands in the TCPP monomer are replaced by a strong peak at 666 nm also with three weak Q-bands in its original TCPP. The distinct bathochromic and hypsochromic shifts by 3 nm in Soret band of the TCPP confirm aggregation formation in comparison with monomeric TCPP, which indicates that most of the TCPP building blocks form *J*-type supramolecular assemblies with induction of arginine [15,37,42]. Similarly, the UV-vis spectrum of GNPs@TCPP nanofibers also show a Soret peak at approximately 420 nm and one strong peak at 666 nm along with three relatively weak peaks in Q-band region. The presence of graphene in this case is responsible for larger bathochromic and hypsochromic shifts, which is

about 6 nm. A broad peak at around 350 nm, which is attributed to the characteristic absorbance of grapheme [43]. The change in the Q-band region is evident in four weak peaks in the absorbance of monomeric TCPP changing to one strong peak along with three relatively weak peaks (inset in Figure 4A) GNPs@TCPP nanofibers. This also support our hypothesis of *J*-type assemblies of TCPP monomers on the GNPs surface.
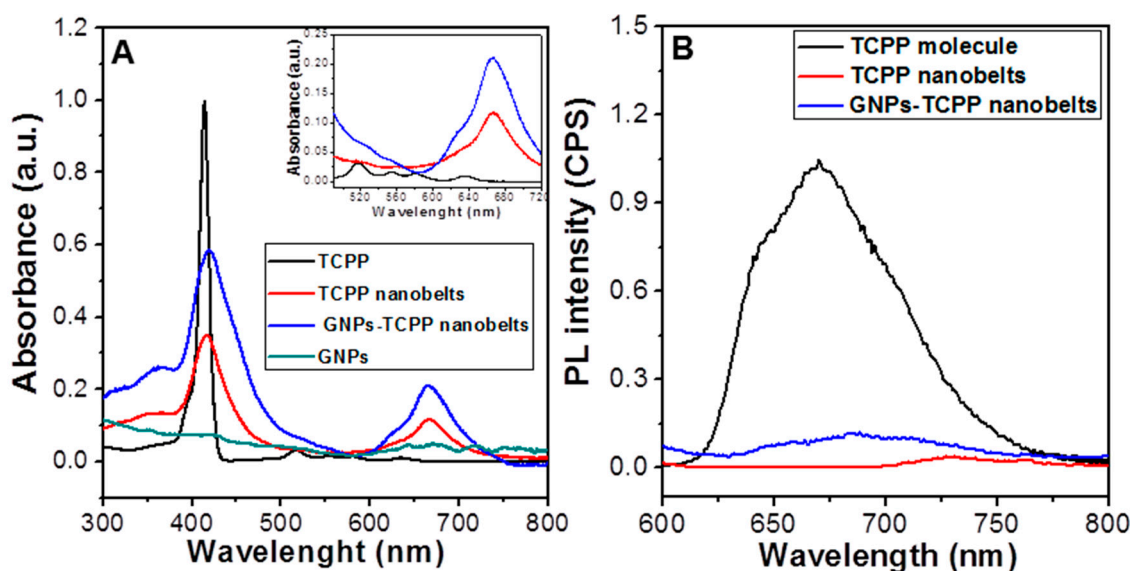

Figure 4. (**A**) and inset of (**A**) UV-vis absorption spectra and (**B**) photoluminescence (PL) spectra of monomeric TCPP molecules (black line), free-standing TCPP nanobelts (red line) and graphene nanoplates (GNP)s@TCPP fibers (blue line).

The optical properties of TCPP nanofibers on GNPs were further investigated by photoluminescence (Figure 4B). The fluorescence spectrum of TCPP in aqueous solution shows one characteristic emission peak at 669 nm. Interestingly, the photoluminescence spectrum of free-standing TCPP nanobelts and GNPs@TCPP nanofibers show relatively weak and broad emission peaks at approximately 730 and 686 nm, respectively. These significant decreases in the emission peaks are likely due to the coupling from the spatial packing of the TCPP porphyrins [26] and the quenching effect of graphene, suggesting an efficient photoinduced process of electron injection from TCPP to GNPs [44].

Figure 5 exhibits XRD patterns of monomeric porphyrin molecules and GNPs@porphyrin nanofibers. There are no peaks observed in the XRD pattern of monomeric TCPP (black line), indicating the non-crystalline nature of the TCPP monomers. However, the XRD pattern of GNPs@TCPP nanofibers (red line) shows several characteristic diffraction peaks of both graphene and TCPP aggregates, while a strong peak at around 26° and a weak peak at 55° are assigned to the graphitic nature of graphene, and other weak diffractions peaks are indexed for TCPP nanofibers. These results indicate that assembled TCPP aggregates are crystalline in nature, which may be due to aromatic π–π stacking between the porphyrin molecules [25]. Fourier transform infrared (FTIR) and Raman spectra of monomeric TCPP and GNPs@TCPP nanofibers also reveal characteristic bands for both GNPs and porphyrin components (Figures S3 and S4) [45].
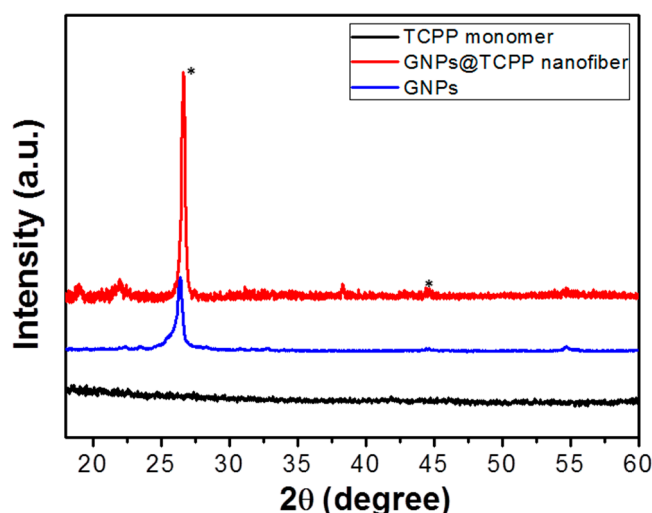
Figure 5. XRD patterns of monomeric TCPP molecule and GNPs@TCPP nanofibers.

TCPP porphyrin aggregates have been demonstrated to have photocatalytic properties in many biological energy transduction processes in plants and algae [46,47]. It has also been confirmed that TCPP aggregates only exhibit photocatalytic properties under visible light [25,27,48]. Thus, in this work, we assess the photocatalytic degradation of Rhodamine B (RhB) and methyl orange (MO) dyes by using GNPs@TCPP nanofibers as a photocatalyst in comparison with GNPs and free-standing TCPP aggregates. The decreases in the absorption peak at 553 and 464 nm of RhB and MO, respectively, as a function of time are monitored to evaluate the photocatalytic performance. Figure 6A,C display the C/C_o versus time plot of RhB and MO under different photocatalytic reaction conditions, where C_o is the initial concentration of dyes and C is the concentration at time t. It is clear in both cases of RhB and MO that with the blank experiment (no photocatalysts), negligible dye degradation could be observed, suggesting that the self-sensitized photodegradation of dyes does not occur under these conditions. When GNPs were used as photocatalyst, while a decrease in RhB concentration of approximately 25% was observed, there is an insignificant decrease in the concentration of MO. This is likely due to good adsorption affinity of graphene toward RhB rather than MO [37]. When using free-standing TCPP aggregate photocatalysts, the concentration of RhB and MO are decreased by 90% and 30% respectively after 180 min of irradiation time under simulated sunlight. This result demonstrates that the free-standing TCPP aggregates display photocatalytic activity toward RhB and MO under visible-light irradiation [23]. Interestingly, the photocatalytic performance increases significantly when GNPs@TCPP nanofibers are used. While RhB is completely degraded after 150 min, MO degradation also reaches 80% after 180 min. These results indicate that GNPs@TCPP nanofibers exhibit enhanced photocatalytic activity in comparison with GNPs and free-standing TCPP aggregates. The photocatalytic activity of GNPs@TCPP nanofibers toward dyes in the dark condition was also tested (Figure S5), which show virtually no photocatalytic activity in this condition, the small decrease in dyes concentration is ascribed to adsorption of dyes by GNPs.

The kinetics of the photocatalytic reaction of RhB and MO by GNPs@TCPP nanofibers are also determined through the plot of ln (A_t/A_0) vs. time, where A_t is the peak intensity at time t, and A_0 is the intensity at time zero (Figure 6B,D). From these plots, the degradation rate constant of RhB and MO by GNPs@TCPP nanofibers as a photocatalyst is calculated to be 15.8×10^{-3} and 6.5×10^{-3} min^{-1}, respectively.
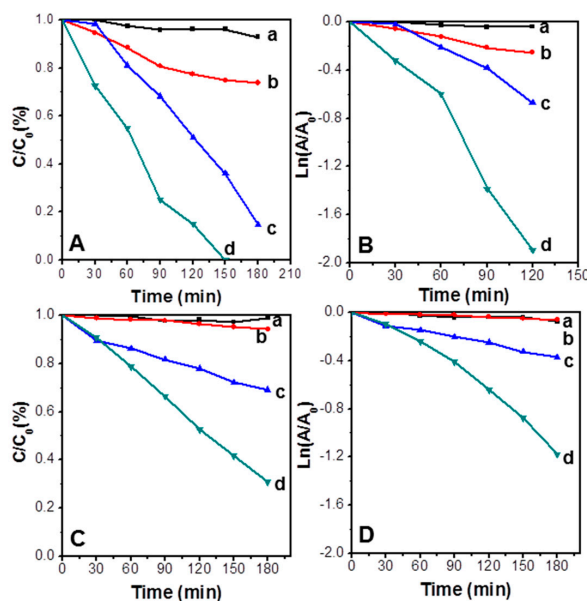
Figure 6. (**A**,**C**) Photocatalytic performance and (**B**,**D**) kinetic simulation curve for RhB and methyl orange degradation, respectively, of (**a**) control without catalyst, (**b**) GNPs, (**c**) free-standing TCPP nanobelts, (**d**) GNPs@TCPP nanofibers.

It is well known that *J*-type porphyrin assemblies can be used as organic semiconductors to harvest light and generate electron-hole pairs under light irradiation [5,42,49,50]. Moreover, previous studies demonstrated that graphene could be used as a support and promoter to improve charge separation, by suppressing the recombination of electron-hole pairs generated from irradiation of the porphyrins, increasing the lifetime of the charge carriers [23,32]. Graphene also plays an important role in enhancing the efficiency of dye adsorption, as it facilitates the interfacial charge transfer to the adsorbed agent [23,51]. Based on this literature, a possible mechanism for the enhanced photocatalytic activity of the GNPs@TCPP nanofibers photocatalyst toward dyes is proposed as illustrated in Figure 7. When a GNPs@TCPP nanofiber is irradiated with visible light, electrons from valence band (VB) of TCPP crystals cross the band gap to the conduction band (CB), resulting in the generation of e^-/h^+ pairs [52]. The generated electron in the CB may move freely to the graphene sheets; consequently, the generated electron-hole pairs are effectively separation and recombination energy is significantly minimized. Dye molecules are oxidized to degraded products on the surface of TCPP nanofibers by active species such as ·OH formed by reaction between photogenerated holes with H_2O or OH^- [24]. On the other side, oxygen in H_2O is reduced on the graphene sheet by the electrons generated from TCPP nanofibers under visible irradiation to form O_3^- radicals [53].
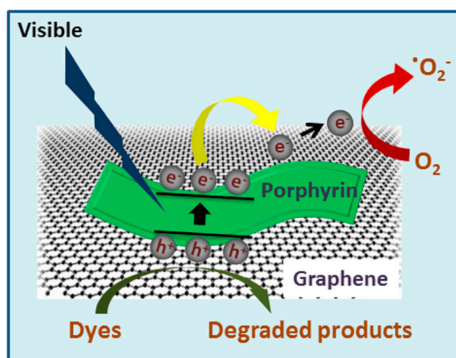

Figure 7. The possible mechanism of the GNPs@TCPP nanofibers photocatalyst for dye degradation.

4. Conclusions

In summary, we have successfully synthesized GNPs@TCPP nanofiber composites by arginine-mediated self-assembly of monomeric molecules on graphene. The resulting TCPP nanofibers are 50–200 nm in diameter with approximately 5 μm in length, being densely and uniformly distributed on the surface of graphene. The GNPs@TCPP nanofiber composite showed enhanced photocatalytic performance compared to free-standing TCPP aggregates under visible-light irradiation, with RhB completely degraded after 150 min. A possible photocatalytic pathway has also been proposed. This study introduces a new promising material, which is a timely contribution to organic/graphene hybrid nanocatalysts, especially useful for applications environmental remediation.

Supplementary Materials: The following are available online: Figure S1, SEM images of the GNPs@TCPP nanofibers composite; Figure S2, TEM images of the GNPs@TCPP nanofibers composite; Figure S3, FTIR spectra of monomeric TCPP molecules and GNPs@TCPP nanofibers; Figure S4; Raman spectra of monomeric TCPP molecules and GNPs@TCPP nanofibers; and Figure S5, photocatalytic performance of GNPs@TCPP nanofibers toward Rhdomine B and methyl orange in the dark condition.

Author Contributions: D.D.L. performed all the experiments and R.V.H. and H.D.N. helped with XRD and XPS analysis; L.A.J. and S.V.B. (IICT) monitored the analysis; S.V.B. (RMIT) supervised the research project. All the co-authors contributed to the manuscript preparation.

Conflicts of Interest: The authors declare no conflict of interest.

References

1. Drain, C.M.; Varotto, A.; Radivojevic, I. Self-organized porphyrinic materials. *Chem. Rev.* **2009**, *109*, 1630–1658. [CrossRef] [PubMed]

2. Auwärter, W.; Écija, D.; Klappenberger, F.; Barth, J.V. Porphyrins at interfaces. *Nat. Chem.* **2015**, *7*, 105–120. [CrossRef] [PubMed]

3. Lee, S.J.; Hupp, J.T. Porphyrin-containing molecular squares: Design and applications. *Chem. Rev.* **2006**, *250*, 1710–1723. [CrossRef]

4. Sakakibara, K.; Hill, J.P.; Ariga, K. Thin-Film-Based Nanoarchitectures for Soft Matter: Controlled Assemblies into Two-Dimensional Worlds. *Small* **2011**, *7*, 1288–1308. [CrossRef] [PubMed]

5. Würthner, F.; Kaiser, T.E.; Saha-Möller, C.R. J-Aggregates: From Serendipitous Discovery to Supramolecular Engineering of Functional Dye Materials. *Angew. Chem. Int. Ed.* **2011**, *50*, 3376–3410. [CrossRef] [PubMed]

6. Lin, Y.; Wang, J.; Zhang, Z.G.; Bai, H.; Li, Y.; Zhu, D.; Zhan, X. An electron acceptor challenging fullerenes for efficient polymer solar cells. *Adv. Mater.* **2015**, *27*, 1170–1174. [CrossRef] [PubMed]

7. Elemans, J.A.; van Hameren, R.; Nolte, R.J.; Rowan, A.E. Molecular Materials by Self-Assembly of Porphyrins, Phthalocyanines, and Perylenes. *Adv. Mater.* **2006**, *18*, 1251–1266. [CrossRef]

8. Hoeben, F.J.; Jonkheijm, P.; Meijer, E.; Schenning, A.P. About supramolecular assemblies of π-conjugated systems. *Chem. Rev.* **2005**, *105*, 1491–1546. [CrossRef] [PubMed]

9. Lehn, J.M. Toward self-organization and complex matter. *Science* **2002**, *295*, 2400–2403. [CrossRef] [PubMed]

10. Xiao, J.; Qi, L. Surfactant-assisted, shape-controlled synthesis of gold nanocrystals. *Nanoscale* **2011**, *3*, 1383–1396. [CrossRef] [PubMed]

11. Lin, C.; Zhu, W.; Yang, H.; An, Q.; Tao, C.A.; Li, W.; Cui, J.; Li, Z.; Li, G. Facile Fabrication of Stimuli-Responsive Polymer Capsules with Gated Pores and Tunable Shell Thickness and Composite. *Angew. Chem. Int. Ed.* **2011**, *123*, 5049–5053. [CrossRef]

12. Jang, J.; Oh, J.H. Facile Fabrication of Photochromic Dye–Conducting Polymer Core–Shell Nanomaterials and Their Photoluminescence. *Adv. Mater.* **2003**, *15*, 977–980. [CrossRef]

13. Cozzoli, P.D.; Pellegrino, T.; Manna, L. Synthesis, properties and perspectives of hybrid nanocrystal structures. *Chem. Soc. Rev.* **2006**, *35*, 1195–1208. [CrossRef] [PubMed]

14. Wang, Z.; Medforth, C.J.; Shelnutt, J.A. Porphyrin nanotubes by ionic self-assembly. *J. Am. Chem. Soc.* **2004**, *126*, 15954–15955. [CrossRef] [PubMed]

15. Guo, P.; Chen, P.; Ma, W.; Liu, M. Morphology-dependent supramolecular photocatalytic performance of porphyrin nanoassemblies: From molecule to artificial supramolecular nanoantenna. *J. Mater. Chem.* **2012**, *22*, 20243–20249. [CrossRef]

16. Lee, S.J.; Hupp, J.T.; Nguyen, S.T. Growth of narrowly dispersed porphyrin nanowires and their hierarchical assembly into macroscopic columns. *J. Am. Chem. Soc.* **2008**, *130*, 9632–9633. [CrossRef] [PubMed]

17. Lee, S.J.; Malliakas, C.D.; Kanatzidis, M.G.; Hupp, J.T.; Nguyen, S.T. Amphiphilic porphyrin nanocrystals: Morphology tuning and hierarchical assembly. *Adv. Mater.* **2008**, *20*, 3543–3549. [CrossRef]

18. Gong, X.; Milic, T.; Xu, C.; Batteas, J.D.; Drain, C.M. Preparation and characterization of porphyrin nanoparticles. *J. Am. Chem. Soc.* **2002**, *124*, 14290–14291. [CrossRef] [PubMed]

19. Hasobe, T.; Oki, H.; Sandanayaka, A.S.D.; Hideyuki, M. Sonication-assisted supramolecular nanorods of meso-diaryl-substituted porphyrins. *Chem. Commun.* **2008**, 724–726. [CrossRef]

20. Gao, Y.; Zhang, X.; Ma, C.; Li, X.; Jiang, J. Morphology-Controlled Self-Assembled Nanostructures of 5, 15-Di [4-(5-acetylsulfanylpentyloxy) phenyl] porphyrin Derivatives. Effect of Metal—Ligand Coordination Bonding on Tuning the Intermolecular Interaction. *J. Am. Chem. Soc.* **2008**, *130*, 17044–17052. [CrossRef] [PubMed]

21. Hu, J.S.; Guo, Y.G.; Liang, H.P.; Wan, L.J.; Jiang, L. Three-dimensional self-organization of supramolecular self-assembled porphyrin hollow hexagonal nanoprisms. *J. Am. Chem. Soc.* **2005**, *127*, 17090–17095. [CrossRef] [PubMed]

22. Medforth, C.J.; Wang, Z.; Martin, K.E.; Song, Y.; Jacobsen, J.L.; Shelnutt, J.A. Self-assembled porphyrin nanostructures. *Chem. Commun.* **2009**, *47*, 7261–7277. [CrossRef] [PubMed]

23. Chen, Y.; Li, A.; Huang, Z.H.; Wang, L.N.; Kang, F. Porphyrin-Based Nanostructures for Photocatalytic Applications. *Nanomaterials* **2016**, *6*, 51. [CrossRef] [PubMed]

24. Chen, Y.; Huang, Z.H.; Yue, M.; Kang, F. Integrating porphyrin nanoparticles into a 2D graphene matrix for free-standing nanohybrid films with enhanced visible-light photocatalytic activity. *Nanoscale* **2014**, *6*, 978–985. [CrossRef] [PubMed]

25. Mandal, S.; Nayak, S.K.; Mallampalli, S.; Patra, A. Surfactant-Assisted Porphyrin Based Hierarchical Nano/Micro Assemblies and Their Efficient Photocatalytic Behavior. *ACS Appl. Mater. Interfaces* **2014**, *6*, 130–136. [CrossRef] [PubMed]

26. Zhong, Y.; Wang, Z.; Zhang, R.; Bai, F.; Wu, H.; Haddad, R.; Fan, H. Interfacial self-assembly driven formation of hierarchically structured nanocrystals with photocatalytic activity. *ACS Nano* **2014**, *8*, 827–833. [CrossRef] [PubMed]

27. La, D.D.; Bhosale, S.V.; Jones, L.A.; Bhosale, S.V. Arginine-induced porphyrin-based self-assembled nanostructures for photocatalytic applications under simulated sunlight irradiation. *Photochem. Photobiol. Sci.* **2017**, *16*, 151–154. [CrossRef] [PubMed]

28. La, D.D.; Bhosale, S.V.; Jones, L.A.; Revaprasadu, N.; Bhosale, S.V. Fabrication of a Graphene@TiO$_2$@ Porphyrin hybrid material and its photocatalytic properties under simulated sunlight irradiation. *ChemistrySelect* **2017**, *2*, 3329–3333. [CrossRef]

29. Zhang, H.; Lv, X.; Li, Y.; Wang, Y.; Li, J. P25-graphene composite as a high performance photocatalyst. *ACS Nano* **2009**, *4*, 380–386. [CrossRef] [PubMed]

30. Gao, N.; Fang, X. Synthesis and Development of Graphene–Inorganic Semiconductor Nanocomposites. *Chem. Rev.* **2015**, *115*, 8294–8343. [CrossRef] [PubMed]

31. Yang, Y.; Han, C.; Jiang, B.; Iocozzia, J.; He, C.; Shi, D.; Jiang, T.; Lin, Z. Graphene-based materials with tailored nanostructures for energy conversion and storage. *Mater. Sci. Eng. R Rep.* **2016**, *102*, 1–72. [CrossRef]

32. Xiang, Q.; Yu, J.; Jaroniec, M. Graphene-based semiconductor photocatalysts. *Chem. Soc. Rev.* **2012**, *41*, 782–796. [CrossRef] [PubMed]

33. Wang, A.; Yu, W.; Huang, Z.; Zhou, F.; Song, J.; Song, Y.; Long, L.; Cifuentes, M.P.; Humphrey, M.G.; Zhang, L. Covalent functionalization of reduced graphene oxide with porphyrin by means of diazonium chemistry for nonlinear optical performance. *Sci. Rep.* **2016**, *6*, 23325. [CrossRef] [PubMed]

34. Kim, S.J.; Song, W.; Kim, S.; Kang, M.A.; Myung, S.; Lee, S.S.; Lim, J.; An, K.S. Tunable functionalization of graphene nanosheets for graphene-organic hybrid photodetectors. *Nanotechnology* **2016**, *27*, 075709. [CrossRef] [PubMed]

35. Stylianakis, M.; Konios, D.; Kakavelakis, G.; Charalambidis, G.; Stratakis, E.; Coutsolelos, A.; Kymakis, E.; Anastasiadis, S. Efficient ternary organic photovoltaics incorporating a graphene-based porphyrin molecule as a universal electron cascade material. *Nanoscale* **2015**, *7*, 17827–17835. [CrossRef] [PubMed]

36. He, Y.; Garnica, M.; Bischoff, F.; Ducke, J.; Bocquet, M.L.; Batzill, M.; Auwärter, W.; Barth, J.V. Fusing tetrapyrroles to graphene edges by surface-assisted covalent coupling. *Nat. Chem.* **2017**, *9*, 33–38. [CrossRef] [PubMed]

37. Guo, P.; Chen, P.; Liu, M. One-dimensional porphyrin nanoassemblies assisted via graphene oxide: Sheetlike functional surfactant and enhanced photocatalytic behaviors. *ACS Appl. Mater. Interfaces* **2013**, *5*, 5336–5345. [CrossRef] [PubMed]

38. La, D.D.; Rananaware, A.; Salimimarand, M.; Bhosale, S.V. Well–dispersed assembled porphyrin nanorods on graphene for the enhanced photocatalytic performance. *ChemistrySelect* **2016**, *1*, 4430–4434. [CrossRef]

39. Zhang, X.; Zhu, B.; Zhou, L.; Liu, P.; Deng, W. Synthesis of Novel Porphyrin Derivatives with Mesogenic Properties. *Syn. Commun.* **2015**, *45*, 2730–2739. [CrossRef]

40. La, M.; Duc, D.; Bhargava, S.; Bhosale, S.V. Improved and a simple approach for mass production of graphene nanoplatelets material. *ChemistrySelect* **2016**, *1*, 949–952. [CrossRef]

41. Sun, J.; Meng, D.; Jiang, S.; Wu, G.; Yan, S.; Geng, J.; Huang, Y. Multiple-bilayered RGO–porphyrin films: From preparation to application in photoelectrochemical cells. *J. Mater. Chem.* **2012**, *22*, 18879–18886. [CrossRef]

42. Kano, H.; Kobayashi, T. Time-resolved fluorescence and absorption spectroscopies of porphyrin J-aggregates. *J. Chem. Phys.* **2002**, *116*, 184–195. [CrossRef]

43. Zhang, Y.; Ma, H.L.; Zhang, Q.; Peng, J.; Li, J.; Zhai, M.; Yu, Z.Z. Facile synthesis of well-dispersed graphene by γ-ray induced reduction of graphene oxide. *J. Mater. Chem.* **2012**, *22*, 13064–13069. [CrossRef]

44. Afzal, S.; Daoud, W.A.; Langford, S.J. Self-cleaning cotton by porphyrin-sensitized visible-light photocatalysis. *J. Mater. Chem.* **2012**, *22*, 4083–4088. [CrossRef]

45. Wan, J.; Wang, H.; Wu, Z.; Shun, Y.C.; Zheng, X.; Phillips, D.L. Resonance Raman spectroscopy and density functional theory calculation study of photodecay dynamics of tetra (4-carboxyphenyl) porphyrin. *Phys. Chem. Chem. Phys.* **2011**, *13*, 10183–10190. [CrossRef] [PubMed]

46. McConnell, I.; Li, G.; Brudvig, G.W. Energy conversion in natural and artificial photosynthesis. *Chem. Biol.* **2010**, *17*, 434–447. [CrossRef] [PubMed]

47. Barber, J. Photosynthetic energy conversion: Natural and artificial. *Chem. Soc. Rev.* **2009**, *38*, 185–196. [CrossRef] [PubMed]

48. La, D.D.; Rananaware, A.; Thi, H.P.N.; Jones, L.; Bhosale, S.V. Fabrication of a TiO$_2$@ porphyrin nanofiber hybrid material: A highly efficient photocatalyst under simulated sunlight irradiation. *Adv. Nat. Sci. Nanosci. Nanotechnol.* **2017**, *8*, 015009.

49. Meadows, P.J.; Dujardin, E.; Hall, S.R.; Mann, S. Template-directed synthesis of silica-coated J-aggregate nanotapes. *Chem. Commun.* **2005**, *29*, 3688–3690. [CrossRef] [PubMed]

50. Kano, H.; Saito, T.; Kobayashi, T. Dynamic intensity borrowing in porphyrin J-aggregates revealed by sub-5-fs spectroscopy. *J. Phys. Chem. B* **2001**, *105*, 413–419. [CrossRef]

51. Chen, Y.; Zhang, C.; Zhang, X.; Ou, X.; Zhang, X. One-step growth of organic single-crystal p–n nano-heterojunctions with enhanced visible-light photocatalytic activity. *Chem. Commun.* **2013**, *49*, 9200–9202. [CrossRef] [PubMed]

52. La, D.D.; Ramanathan, R.; Rananaware, A.; Bansal, V.; Bhosale, S.V. Nanostructured charge transfer complex of CuTCNQF 4 for efficient photo-removal of hexavalent chromium. *RSC Adv.* **2016**, *6*, 33931–33936. [CrossRef]

53. Li, D.; Dong, W.; Sun, S.; Shi, Z.; Feng, S. Photocatalytic degradation of acid chrome blue K with porphyrin-sensitized TiO$_2$ under visible light. *J. Phys. Chem. C* **2008**, *112*, 14878–14882. [CrossRef]